

6 Physics of Single Quantum Emitters

Highlights of this chapter: In this chapter, first the concepts of and properties of different light states, especially single-photons are discussed. We also review single-photon sources with a focus on diverse quantum emitters and their properties.

6.1 Introduction

In the past decades, single quantum emitters have become a manifold tool for the development of new light sources, such as lasers, LEDs, and single-photon sources, for nano-electronic devices, but also in chemistry and life sciences where they act as nanoscopic probes and labels. Especially in the emerging field of quantum information processing, quantum emitters are utilized as sources for single photons or as stationary quantum bits.

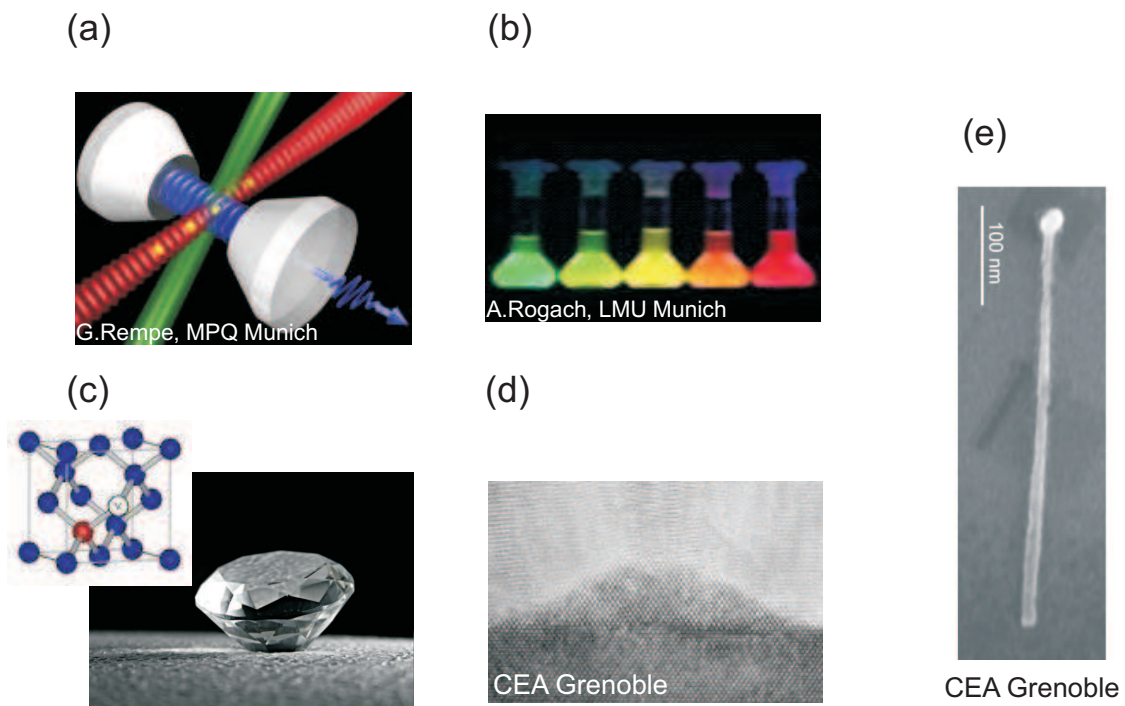


Figure 152: Examples of quantum emitters: (a) single atom in a high-finesse cavity, (b) colloidal nanocrystals of different size. (c) nitrogen–vacancy defect centre in diamond, (d) TEM image of a CdSe/ZnSe quantum dot, (e) TEM image of a CdSe/ZnSe nanowire quantum dot structure.

6.2 Photon Statistics and Single Photon States

In the year 1905, Albert Einstein published his ingenious explanation of the photoelectric effect, for which he was rewarded with the Nobel Prize in Physics in 1921. In this work he explained the emission of electrons from a metal plate by the absorption of light particles, which is in opposition to the classical wave picture. Until today, the photon is a workhorse to test the foundations of quantum physics against recurring efforts of a purely classical interpretation of nature.

6.2.1 Brief review of quantization of the electromagnetic field

Here we will briefly review the quantization of the electro-magnetic field that leads to the concept of photons.

Starting point are the source-free Maxwell equations:

$$\operatorname{div} \mathbf{D} = \rho \quad (278)$$

$$\operatorname{div} \mathbf{B} = 0 \quad (279)$$

$$\operatorname{rot} \mathbf{E} = -\partial \mathbf{B} / \partial t \quad (280)$$

$$\operatorname{rot} \mathbf{H} = \mathbf{J} + \partial \mathbf{D} / \partial t, \quad (281)$$

A convenient gauge is the Coulomb gauge:

$$\mathbf{B} = \operatorname{rot} \mathbf{A} \quad (282)$$

$$\mathbf{E} = -\partial \mathbf{A} / \partial t \quad (283)$$

$$\operatorname{div} \mathbf{A} = 0 \quad (284)$$

for which the vector potential obeys the wave equation

$$\Delta \mathbf{A}(\mathbf{r}, t) = \frac{1}{c^2} \partial^2 \mathbf{A}(\mathbf{r}, t) / \partial t^2 \quad (285)$$

For the vector potential \mathbf{A} , we make the ansatz

$$\mathbf{A}(\mathbf{r}, t) = \sum_{k,\lambda} \sqrt{\frac{\hbar}{2\omega_K \epsilon_0}} (a_{k,\lambda} \mathbf{u}_{k,\lambda}(\mathbf{r}) e^{-i\omega_k t} + a_{k,\lambda}^* \mathbf{u}_{k,\lambda}^*(\mathbf{r}) e^{+i\omega_k t}) \quad (286)$$

Here we sum over all wave vectors $\mathbf{k} = (k_x, k_y, k_z)$ and have split \mathbf{A} into a positive and a negative frequency part. The mode functions $\mathbf{u}_k(\mathbf{r})$ also obey the wave equation (285) and form a complete ortho-normal basis:

$$\int_V \mathbf{u}_k^*(\mathbf{r}) \cdot \mathbf{u}_{k'}(\mathbf{r}) d^3 r = \delta_{k,k'}$$

The mode functions depend on the boundary conditions of the physical volume V under consideration. E.g. in a cubic volume of size $V = L^3$,

$$\mathbf{u}_k(\mathbf{r}) = L^{-3/2} \mathbf{e}_\lambda e^{i\mathbf{k}\cdot\mathbf{r}}$$

where \mathbf{e}_λ is the unit polarization vector and $\lambda = 1, 2$. Each component of the wave vector takes the values $k_{x,y,z} = 2\pi n_{x,y,z}/L$, with $i = (x, y, z)$ and $n_{x,y,z} = (0, \pm 1, \pm 2, \dots)$.

The *Quantization* of the electromagnetic field is performed by replacing the complex Fourier coefficients in (286) with adjungated operators, in analogy of the quantization of the harmonic oscillator:

$$a_{k,\lambda} \rightarrow \hat{a}_{k,\lambda} \quad (287)$$

$$a_{k,\lambda}^* \rightarrow \hat{a}_{k,\lambda}^\dagger \quad (288)$$

The electric field then becomes

$$\hat{\mathbf{E}} = \hat{E}^{(+)} + \hat{E}^{(-)} \quad (289)$$

$$= i \sum_{k,\lambda} \sqrt{\frac{\hbar\omega_k}{2\epsilon_0 V}} \mathbf{e}_\lambda \left(\hat{a}_{k,\lambda} e^{i(\mathbf{k}\cdot\mathbf{r} - \omega_k t)} + \text{h.c.} \right) \quad (290)$$

where $E^{(\pm)}$ is the positive (negative) frequency term.

(in the following, we will omit the hat that indicates the operator: $\hat{a} \rightarrow a$. Furthermore we will collect the indices for wavevector and polarization into one index $(k, \lambda) \rightarrow k$. If we refer to only one mode, this index will be completely omitted.)

These operators obey the commutation relations

$$[a_k, a_{k'}] = [a_k^\dagger, a_{k'}^\dagger] = 0 \quad (291)$$

$$[a_k, a_{k'}^\dagger] = \delta_{k,k'} \quad (292)$$

and the Hamiltonian of the electro-magnetic field becomes analogous to that of an harmonic oscillator:

$$\mathcal{H} = \frac{1}{2} \int \left(\epsilon_0 |\mathbf{E}|^2 + \mu_0 |\mathbf{H}|^2 \right) \quad (293)$$

$$= \sum_k \hbar\omega_k \left(a_k^\dagger a_k + \frac{1}{2} \right) \quad (294)$$

In quantum optics one distinguishes basically the following states.

Fock or Number States

The eigenstates of the Hamiltonian of the free electromagnetic field are $|n_k\rangle$ with positive integer eigenvalues $n_k = (0, 1, 2, \dots)$:

$$a_k^\dagger a_k |n_k\rangle = n_k |n_k\rangle$$

The operator $N = a_k^\dagger a_k$ is Hermitian and is called *number operator*, the eigenstates $|n\rangle$ are called *number states* or *Fock states*. Fock states represent states with an defined number of excitations (here photons).

The operators a_k and a_k^\dagger have the following effect on Fock states:

$$a_k |n_k\rangle = \sqrt{n_k} |n_k - 1\rangle \quad (295)$$

$$a_k^\dagger |n_k\rangle = \sqrt{n_k + 1} |n_k + 1\rangle \quad (296)$$

Thus, a^\dagger and a are called *creation* and *annihilation operators*, respectively.

Using creation operators, each Fock state can be constructed from the vacuum state $|0\rangle$ by

$$|n_k\rangle = (n_k!)^{-1/2} (a_k^\dagger)^{n_k} |0\rangle$$

Furthermore, Fock states form an complete orthonormal basis in the Hilbert space: $\langle n_k | m_k \rangle = \delta_{m,n}$ and $\sum_k |n_k\rangle \langle n_k| = 1$.

Coherent States

A further important class of states are *coherent states*, $|\alpha\rangle$. They are defined as the eigenstates of the annihilation operator:

$$a|\alpha\rangle = \alpha|\alpha\rangle$$

with a complex eigenvalue $\alpha \in \mathbb{C}$.

Coherent states can be expanded in the Fock basis:

$$|\alpha\rangle = e^{-|\alpha|^2/2} \sum_n \frac{\alpha^n}{\sqrt{n!}} |n\rangle$$

Coherent states are *not* orthogonal: $\langle \alpha | \beta \rangle = \exp(-|\alpha - \beta|^2)$ and it holds: $\iint |\alpha\rangle \langle \alpha| d^2\alpha = \pi > 1$. Coherent states are *overcomplete*.

An important property of coherent states is, that they possess a Poissonian photon number probability distribution:

$$P(n) = |\langle n | \alpha \rangle|^2 = e^{-|\alpha|^2} \frac{|\alpha|^{2n}}{n!}$$

with mean photon number

$$\langle n \rangle = \langle \alpha | a^\dagger a | \alpha \rangle = |\alpha|^2$$

Coherent states especially describe the state of a laser field above threshold. One can show that in case of coherent states, the equations of motion for the expectation values of operators correspond with that of classical observables. Coherent thus represent 'classical' states.

Thermal States

A third class of quantum states of light are thermal states. These states are produced by thermal sources, e.g. a light bulb or a discharge lamp.

The photon number distribution of a thermal state is:

$$p(n) = \frac{1}{1 + \bar{n}} \left(\frac{\bar{n}}{1 + \bar{n}} \right)^n \quad (297)$$

This follows directly from the Boltzmann distribution:

$$p(n) = \frac{\exp(-E_n/k_B T)}{\sum_n \exp(-E_n/k_B T)} \quad (298)$$

The mean number of photons in a thermal state obeys a Planck-distribution:

$$p(n) = \frac{1}{e^{\hbar\omega/k_B T} - 1} \quad (299)$$

The density operator of a thermal state is:

$$\rho_{thermal}(n) = \sum_n \frac{\bar{n}^n}{\bar{n}^{n+1}} |n\rangle \langle n| \quad (300)$$

Figure 153 shows the photon number distribution for a thermal and a coherent state. Obviously, the thermal state has a wider photon number distribution.

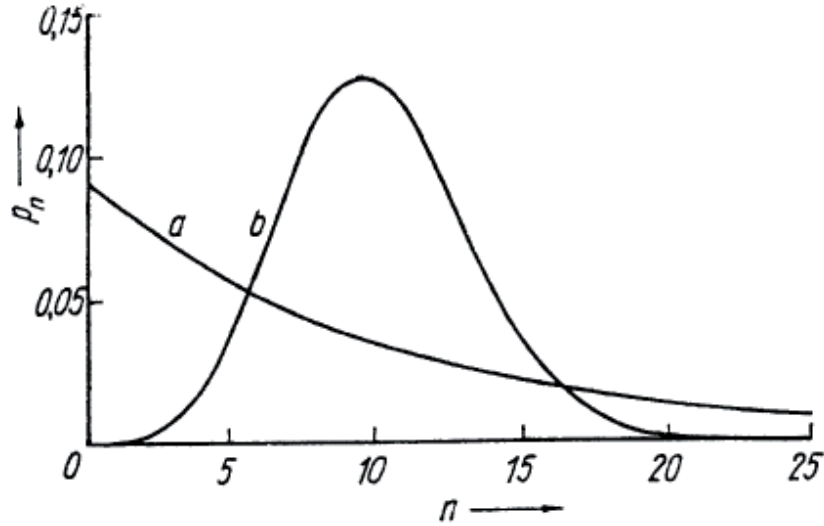


Figure 153: Photon number representation of a thermal state (a) and a coherent state (b) for $\bar{n} = 10$

6.2.2 Coherence functions

An important tool for characterizing the statistical properties of electro-magnetic fields are correlation functions. The general definition for the coherence function of order n is

$$G^{(n)}(x_1, \dots, x_n; x_{n+1}, \dots, x_{2n}) = \langle E^{(-)}(x_1) \dots E^{(-)}(x_n) E^{(+)}(x_{n+1}) \dots E^{(+)}(x_{2n}) \rangle$$

Depending on the physical problem x describes spatial (\mathbf{r}) or temporal (t) coordinates.

First Order Coherence

The first order coherence function

$$G^{(1)}(x_1; x_2) = \langle E^{(-)}(x_1) E^{(+)}(x_2) \rangle$$

describes the interference of light. As an example, consider the interference of two point sources at $\mathbf{r}_{1,2}$ on a screen at position \mathbf{r} (Young's double slit experiment), figure 154.

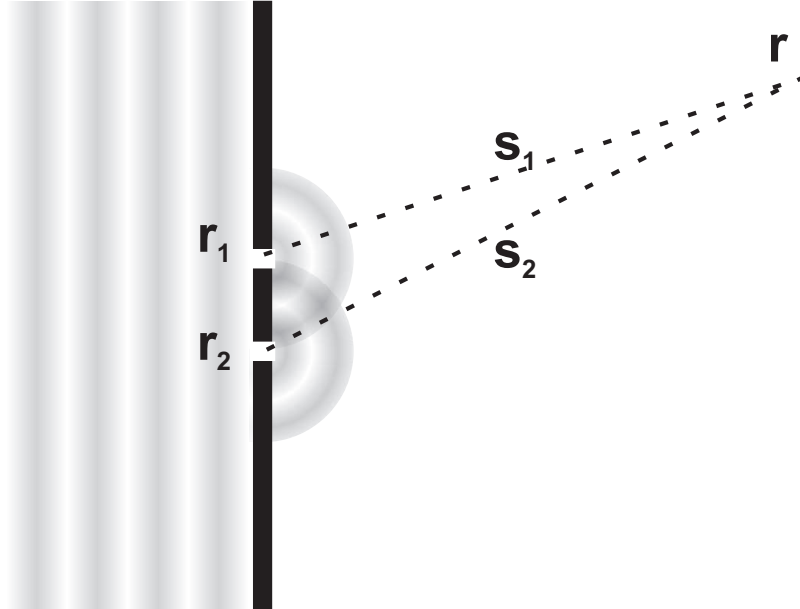


Figure 154: Interference of two spherical waves on a screen.

The electric fields emerging from each slit 1 and 2 are given by

$$E_{1,2}^{(+)}(\mathbf{r}, t) = E_{1,2}^{(+)}(\mathbf{r}_{1,2}, t - s_{1,2}/c) \frac{R_s}{s_{1,2}}$$

where $s_{1,2} = |\mathbf{r} - \mathbf{r}_{1,2}|$ and R_s is some constant (here depending on the slit size).

The total field at \mathbf{r} is

$$E^{(+)}(\mathbf{r}, t) = E_1^{(+)}(\mathbf{r}, t) + E_2^{(+)}(\mathbf{r}, t) \quad (301)$$

$$\approx \frac{R_s}{s} \left(E_1^{(+)}(\mathbf{r}_1, t) + E_2^{(+)}(\mathbf{r}_2, t) \right) \quad (302)$$

The second line holds for closely separated slits with $s \approx s_{1,2} \gg |\mathbf{r}_1 - \mathbf{r}_2|$ and after inserting the field emerging from slit 1 and 2, respectively.

With the abbreviation $x_{1,2} = (\mathbf{r}_{1,2}, t)$, the intensity at $x = (\mathbf{r}, t)$ becomes

$$I = \langle E_1^{(-)}(x)E_1^{(+)}(x) \rangle \quad (303)$$

$$= G^{(1)}(x_1; x_1) + G^{(1)}(x_2; x_2) + 2\text{Re} [G^{(1)}(x_1; x_2)] \quad (304)$$

$$= G^{(1)}(x_1; x_1) + G^{(1)}(x_2; x_2) + 2|G^{(1)}(x_1; x_2)| \cos \phi(x_1, x_2) \quad (305)$$

where $\phi(x_1, x_2)$ is the phase of $G^{(1)}(x_1; x_2)$. One sees that the oscillating term can be identified with the first order coherence function.

If $G^{(1)}(x_1; x_2)$ factorizes, i.e.

$$G^{(1)}(x_1; x_2) = \epsilon^{(-)}(x_1)\epsilon^{(+)}(x_2)$$

the field is called *coherent in first order*. This is especially the case for coherent states $|\alpha\rangle$ which are even coherent in any order and thus motivating their name. Fock states are coherent in first order *only*.

In the temporal domain and for stationary fields, the coherence function is given by

$$G^{(1)}(t, t + \tau) \equiv G^{(1)}(\tau) = \langle E^{(-)}(0)E^{(+)}(\tau) \rangle$$

This function is related to the spectrum of the electro-magnetic field via its Fourier transform:

$$S(\omega) = \int_{-\infty}^{\infty} d\tau e^{-i\omega\tau} G^{(1)}(\tau)$$

Second Order Coherence Function

The second order coherence function is an important tool for the characterization of the non-classical features of quantum states. In the temporal domain and for stationary fields it is given by

$$G^{(2)}(\tau) = \langle E^{(-)}(0)E^{(-)}(\tau)E^{(-)}(\tau)E^{(-)}(0) \rangle$$

Often, one considers with the *normalized* second order coherence function

$$g^{(2)}(\tau) = \frac{G^{(2)}(\tau)}{G^{(2)}(0)} \quad (306)$$

$$= \frac{\langle a^\dagger(0)a^\dagger(\tau)a(\tau)a(0) \rangle}{\langle (a^\dagger(0)a(0))^2 \rangle} \quad (307)$$

One can distinguish the following cases (see also figure 155):

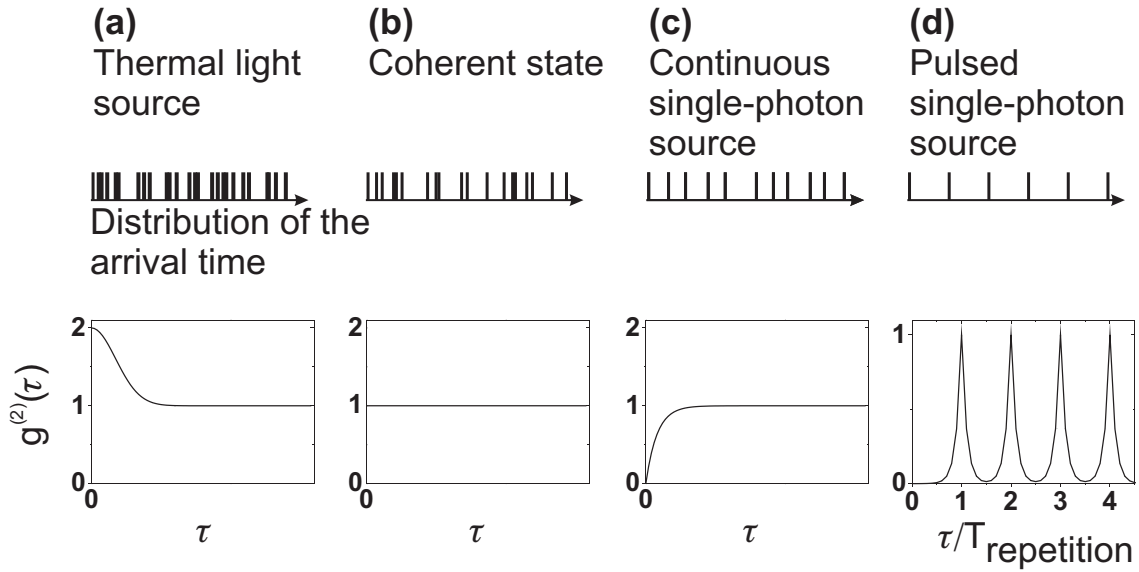


Figure 155: Example of the second order coherence function of different states.

- **Coherent fields:** For coherent light (i.e. coherent states $|\alpha\rangle$), $G^{(2)}(\tau)$ factorizes and $g^{(2)}(\tau) \equiv 1$ for all τ .

This can be interpreted in a way that photons in such a light field appear completely uncorrelated from each other (e.g. as seen by a photo detector). In this special case, the field is referred to as coherent in second order.

- **Bunching:** For classical, fluctuating light (from ensembles of emitters or thermal states) one can generally show:

$$g^{(2)}(\tau) = 1 + |g^{(1)}(\tau)|^2 \geq 1 \quad \text{and} \quad (308)$$

$$g^{(2)}(0) \geq g^{(2)}(\tau) \quad (309)$$

For example, light with a Lorentz spectrum obeys $g^{(2)}(\tau) = 1 + \exp(-\gamma\tau)$. As the width of the bunching peak is approximately the inverse of the spectral bandwidth, bunching of thermal sources can only be observed when the coherence length is smaller than the time resolution of the detectors.

The physical interpretation of this *bunching* phenomena is, that in classical light sources and due to the bosonic character photons tend to appear in bunches.

- **Antibunching:** In case of photon number states $|n\rangle$, the inverse result is

observed, a reduced coherence function at $\tau = 0$:

$$g^{(2)}(0) = 1 - \frac{1}{n}$$

Antibunching cannot be explained by purely classical theories and is thus a quantum mechanical effect. In an analogous way as before, the interpretation is, that the presence of a photon statistically reduces the probability for a second one in the same time bin.

In the special case of a single-photon state $g^{(2)}(0) = 0$.

The first direct measurement of antibunching was performed in 1977 by H.J. Kimble et al., when investigating the photon statistics in the fluorescence of an Na atom beam, see figure 156.

In the case of a pulsed source, the second order coherence function possesses a peaked structure. Here, a missing peak at $\tau = 0$ indicates the generation of only one photon per pulse.

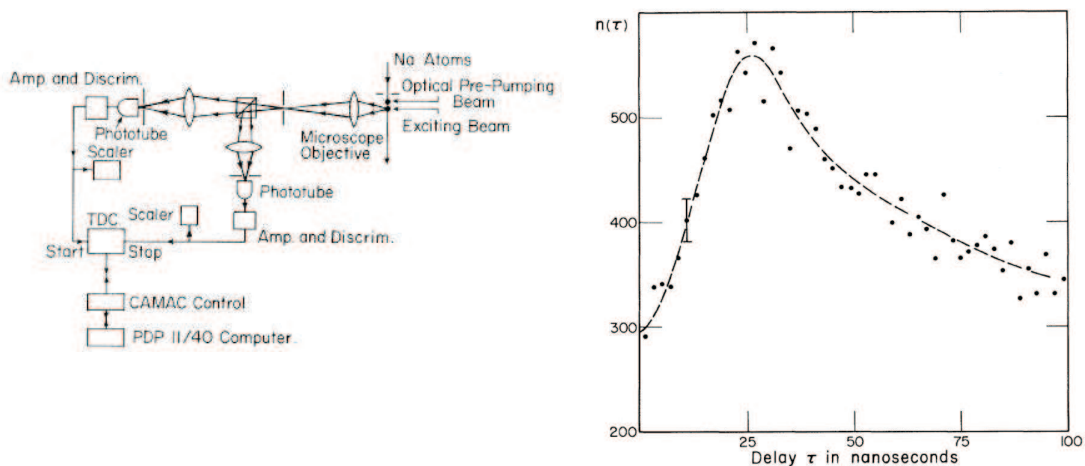


Figure 156: Left: Outline of the principle elements of the experiment by Kimble. Right: The number of recorded pulse pairs as a function of the delay time τ . See also section about Hanbury Brown-Twiss measurements. [Kimble et al., PRL 39, 691]

Measurement of the Second Order Coherence Function

The straightforward method to measure the second order coherence function would be to simply note the times of the detection events at the photodetector and to

explicitly compute the correlation function. However, this approach prevents the measurement of time scales smaller than the detectors dead time. For example, avalanche photodetector modules, which offer the highest detection efficiencies in the visible spectrum, have typical dead times around 50 ns.

To overcome this problem, the arrangement in figure 157, using *two* photodetectors monitoring the outputs of a 50:50 beam splitter, is chosen. Such a setup was originally used by Hanbury Brown and Twiss to detect the spatial correlation function, with which they determined the diameter of stars (Hanbury Brown and Twiss, Nature 178, 1046 (1956)). With the Hanbury Brown-Twiss arrangement, the second detector can be armed right after the detection event of the first.

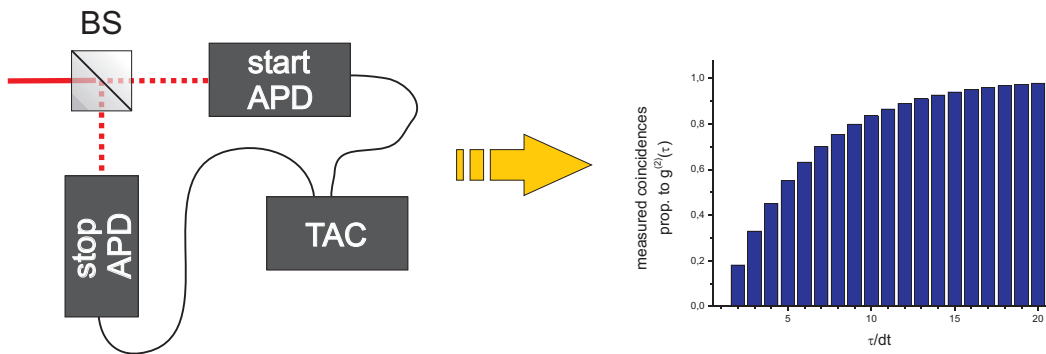


Figure 157: Measurement of the second order coherence function with a Hanbury Brown-Twiss setup. BS: Beam splitter, TAC: time amplitude converter, APD: avalanche photo detector.

Technically, it is very difficult to acquire absolute detection times with a resolution in the nanosecond regime. Instead, only the time differences between the detection events are usually registered and binned together in a histogram (see right part of figure 157). Using a time-to-amplitude converter, time differences can be measured very precisely. The such measured distribution of coincidences is proportional to $g^{(2)}(\tau)$ in the limit of low count rates ($\tau \ll$ average time between two detection events).

6.3 Generation of Single-Photon States with Single Quantum Emitters

There are different ways to realize single photon sources:

1. **attenuated laser pulses:** The easiest way to approximate single-photon states is to use highly attenuated laser pulses: Due to their Poissonian pho-

ton number distribution, the relative amount of multi-photon probability scales linear with the mean photon number

$$P(n \geq 2)/P(n = 1) \approx \mu \quad (310)$$

which approximates (!) a single-photon state for a mean photon number $\mu \ll 1$. However, the single-photon efficiency scales in the same way, ($P(n = 1) \approx \mu$) for $\mu \ll 1$, which makes this method highly inefficient. Also the probability to find more than one photon per time interval cannot be neglected.

2. **heralded single photons:** A widely used alternative is parametric down-conversion, where a non-linear crystal is pumped by a strong laser field (see figure 158). With a certain probability, a laser photon is down-converted to a photon-pair of half frequency. The detection of the first photon heralds the presence of the second with a high accuracy. As this is a random process, no on-demand single-photon generation can be achieved.

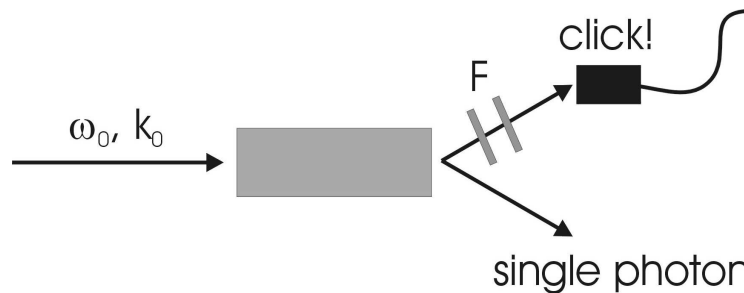


Figure 158: Principle of (non-deterministic) single photon generation. F is a set of filters.

3. **single quantum systems:** A quantum emitter is generally defined as a quantum system that is capable of radiative optical transitions. When observing the spontaneous decay of a single excited quantum emitter, the emission of a single photon is expected. When suppressing non-radiative decay mechanisms, they can principally act as 100% efficient single-photon sources. The variety of systems offered by nature allows a multitude of possible experiments and implementations of photonic applications.

6.3.1 Atoms and Ions

Discrete electronic transitions in atoms are the most self-evident systems for single photon generation. In recent experiments, single atoms or single ions were coupled

to high-finesse cavities to control the emission time and mode of the photon. An example is shown in figure 159. The emission of an isolated single atom is characterized by a high mode purity, which is important for experiments based on two-photon interference. Atom decay cascades can also be used for entangled photon generation. However, the complexity of today's atom traps restricts this system to fundamental experiments.

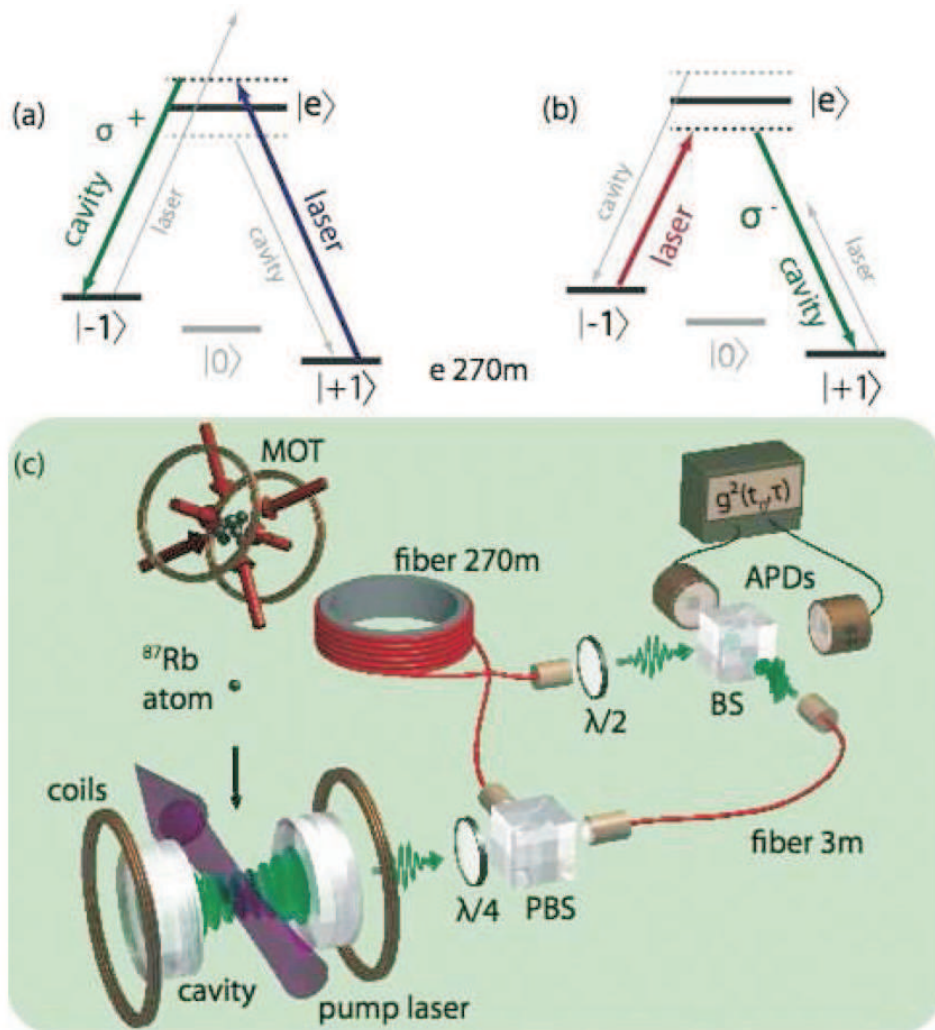


Figure 159: Experiment by Rempe et al., PRL 98, 063601 (2007). The top shows relevant energy levels in ^{87}Rb for single photon generation. (a) The pump laser and cavity drive a resonant Raman transition which takes the atom from $|+1\rangle$ to $|-1\rangle$, producing a σ^+ photon. (b) A second pump pulse of different frequency returns the atom to $|+1\rangle$, thereby producing a σ^- photon. (c) As atoms fall from a magneto-optical trap (MOT) through the cavity the pump laser is inserted from the side to generate photons. The photons are directed through one of two fibers by a polarizing beam splitter (PBS), the long 270-m fiber acting as a delay line. Photons emerging from the fibers can interfere at a beamsplitter (BS), and are detected by a pair of avalanche photodiodes (APDs).

6.3.2 Epitaxial Quantum Dots

Quantum dots are intermediate systems on the evolution from a single atom to a solid. They are semiconductor structures with very small spatial dimensions, surrounded by higher band-gap material. In such a system, electrons in the conduction band and holes in the valence band are strongly confined in all three spatial dimensions. This leads to a discretization of the energy level scheme, which makes quantum dots in many ways similar to atoms rather than to bulk semiconductors.

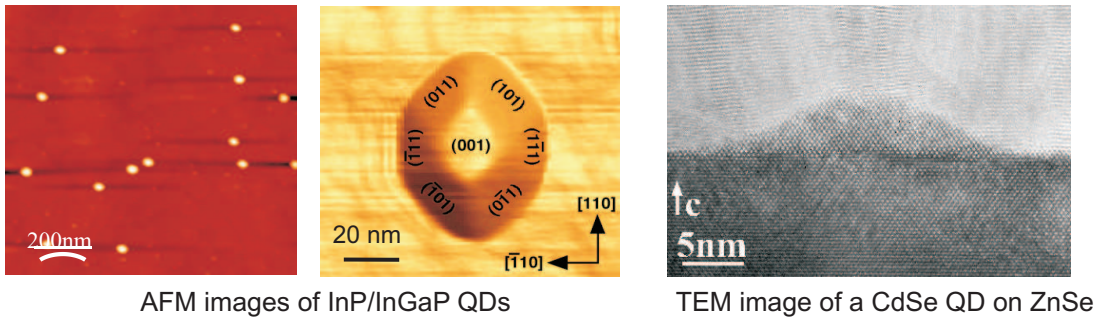


Figure 160: Examples of epitaxial quantum dots (QDs) [HU Berlin & CEA Grenoble].

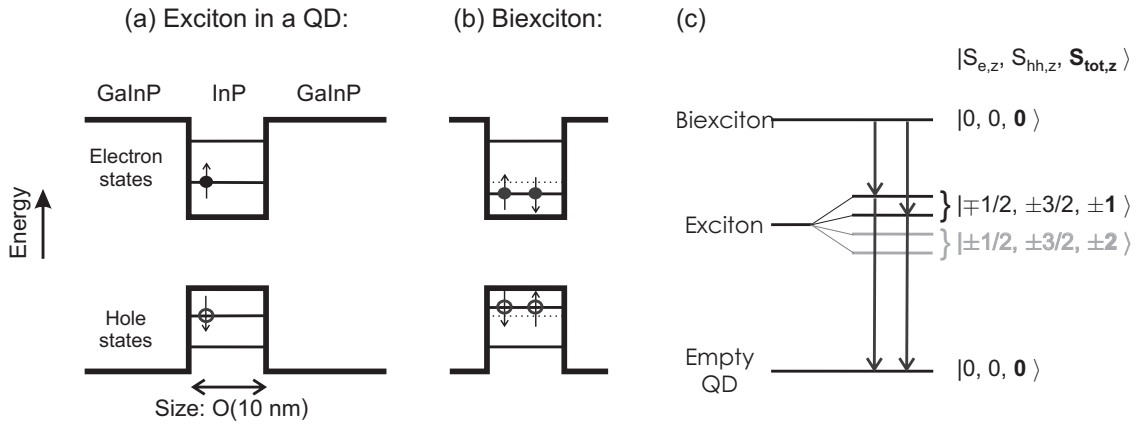


Figure 161: Excitations in a quantum dot: (a) Exciton formed by an electron-hole pair, (b) The biexciton containing two electron-hole pairs with generally a different energy than the exciton. (c) Schematic term scheme for the exciton and biexciton decay cascade. The two dark excitons are indicated by gray lines.

Figure 161 shows the schematical band diagram of a quantum dot (the energies are not in scale). Electrons and holes in the heterostructure (e.g. made by InP/InGaP) see a rectangular potential. In the effective mass approximation, the wave function of a single electron in the conduction band, which experiences a slowly varying potential, is given by:

$$\psi_e(\mathbf{r}) = \Phi(\mathbf{r})u(\mathbf{r})$$

where the Bloch function $u(\mathbf{r})$ is periodic with the lattice periodicity. The slowly varying envelope function $\Phi(\mathbf{r})$ obeys the Schrödinger equation

$$\left(-\frac{\hbar^2}{2} \nabla \frac{1}{m^*} \nabla + V(\mathbf{r}) \right) \Phi(\mathbf{r}) = E\Phi(\mathbf{r})$$

where m^* is the effective electron mass in the respective medium.

As an example, we consider a spherical quantum dot of radius R_0 with finite barriers, where the effective potential has the form:

$$V(r) = \begin{cases} -V_0 & , r \leq R_0 \\ 0 & , r > R_0 \end{cases}$$

The wavefunction can be separated into radial and angular components

$$\phi(\mathbf{r}) = R_{nml}(r)Y_{lm}(\theta, \varphi)$$

where $Y_{lm}(\theta, \varphi) = \sqrt{(2l+1)(l-m)!/[4\pi(l+m)!]} \exp(im\varphi)P_{lm}(\cos\theta)$ are the spherical harmonic functions and P_{lm} are associated Legendre polynomials.

For the ground state ($n = 1$), the angular momentum $l = 0$ and the solution for the wavefunction is

$$R(r) = \begin{cases} \frac{\sin(kr)}{kr} & , r \leq R_0 \\ \frac{\sin(kR_0)}{kR_0} \exp[-\kappa(r - R_0)] & , r > R_0 \end{cases} \quad (311)$$

$$k^2 = 2m_1^*(V_0 + E)/\hbar^2 \quad (312)$$

$$\kappa^2 = -2m_2^*E/\hbar^2 \quad (313)$$

Outside the potential, the wavefunction decays exponentially.

The energies for the ground state and the first excited state are given by the transcendental equations

$$\text{ground state:} \quad kR_0 \cot(kR_0) = 1 - \frac{m_1^*}{m_2^*}(1 + \kappa R_0) \quad (314)$$

$$\text{1}^{\text{st}}\text{exc. state:} \quad kR_0 \cot(kR_0) = 1 + \frac{k^2 R_0^2}{\frac{m_1^*}{m_2^*} \frac{2+2\kappa R_0 + \kappa^2 R_0^2}{1+\kappa R_0} - 2} \quad (315)$$

In the case of infinite barriers ($V_0 \rightarrow \infty$), the wavefunction vanishes outside the quantum dot and is given by (normalized)

$$R_{nml}(r) = \sqrt{2/R_0^3} \frac{j_l(k_{nl}r)}{j_{l+1}(k_{nl}R_0)}$$

where k_{nl} is the n -th zero of the Bessel function j_l . The $(2l + 1)$ degenerate energy levels are

$$E_{nl} = \frac{\hbar^2}{2m^*} \frac{k_{nl}^2}{R_0^2}$$

The 1s, 1p, and 1d states have smaller eigenenergies than the 2s state.

It can be seen from this example that only discrete energies are allowed, comparable to the situation in atoms. For finite barriers and small sizes, only the first few states are considered, while above the potential barrier a continuum of energy levels is present. Although, here, many simplifications were made compared to more realistic dot geometries, this model is suitable to give a qualitative understanding and to demonstrate the discrete energy scheme.

When the quantum dot is occupied with several electrons or holes, Coulomb interaction has to be taken into account. While equally charged carriers suffer a repulsion, for an electronhole pair the energy of the system is lowered and an *exciton* is formed (figure 161(a)). The recombination of the exciton leads to the emission of a single photon.

In the same way, two electron-hole pairs form a *biexciton*, but with in general different energy due to Coulomb interaction (figure 161(b)). When decaying, first one electronhole pair recombines, which leads to the emission of one photon and to a remaining exciton in the quantum dot, which can lead to a second emission of a photon with different wavelength (figure 161(c)).

Due to the Pauli exclusion principle, each electron state can be occupied by at most two electrons corresponding to the two spin states $S_{e,z} = \pm 1/2$. In low dimensional systems the dispersion relation is changed with respect to a bulk crystal, so that heavy holes (with $S_{hh,z} = \pm 3/2$) possess a lower energy than light holes ($S_{lh,z} = \pm 1/2$). Thus, in the lowest state, the quantum dot can also be occupied by only two holes leading to four combinations of the electron and hole spin in the exciton ground state with total spin $S_{tot,z} = \pm 2, \pm 1$. In the biexciton ground state both spin states of the electrons and holes are occupied, resulting in a single state with $S_{tot,z} = 0$. As for radiative transitions, the change of spin has to be carried away by the photon, two of the exciton states (with total spin ± 2) are dark states and participate neither in the biexciton nor the exciton decay, as symbolized in figure 161(c).

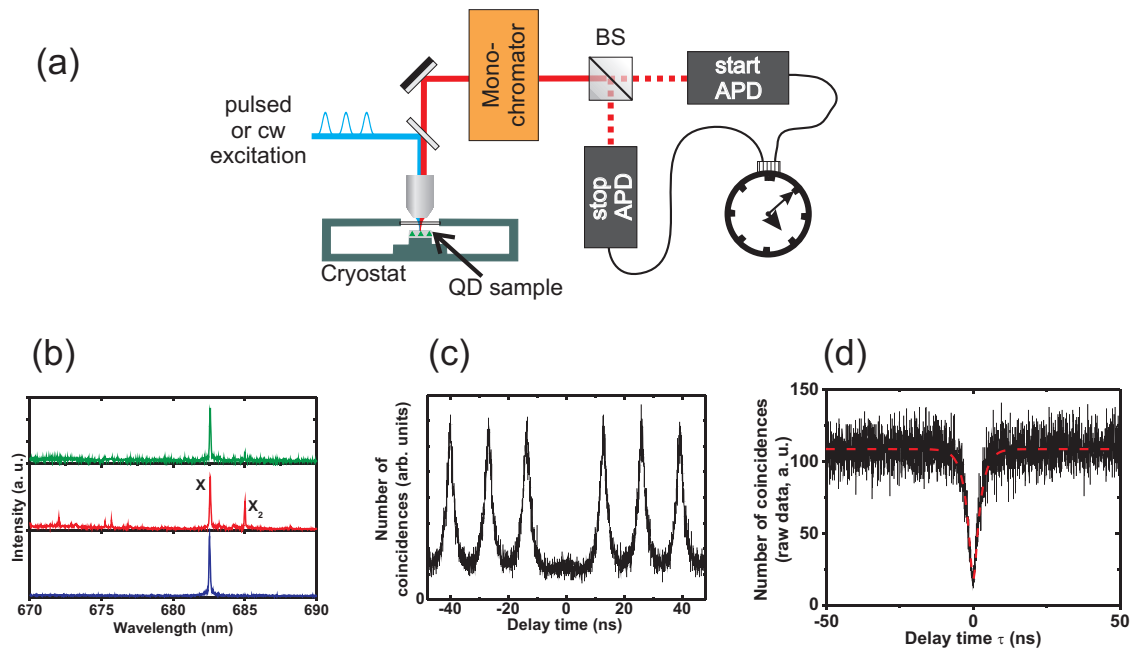


Figure 162: (a) Typical μ -PL setup for single QD experiments. (b) Spectrum of a single InP/InGaP QD at low (top) and high (centre) excitation power and after filtering the exciton (X) from the biexciton (X₂) line (bottom). (c) & (d) Second order coherence function under pulsed and cw excitation, respectively. [HU Berlin, Zwiller et al., APL 82, 1509 (2003)]

Similar to single atoms, single quantum dots can be excited optically (e.g. into excited states or into the continuum above bandgap). Typically carriers relax very quickly into the exciton ground state from where spontaneous single-photon emission can occur. In order to suppress phonon interactions and thermal escape, quantum dots have to be cryogenically cooled (typ. <100 K, but single-photon emission was recently observed at 220 K in CdSE/ZnSe nanowire QDs). Figure 162 shows such an experiment.

The decay cascade of biexciton–exciton–ground state can even lead to the emission of entangled photon pairs. This is shown in figure 163.

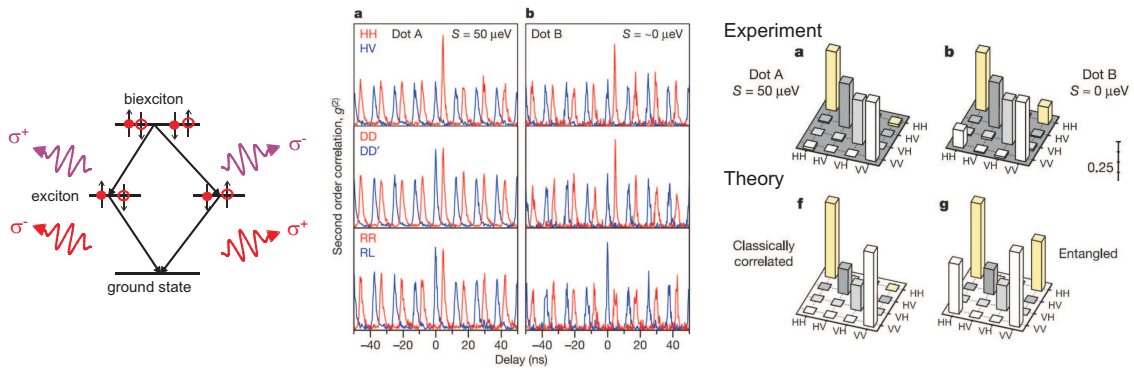


Figure 163: Left: principle of entangled photon pair generation with a QD. Centre: Cross-correlation functions of an unentangled (left graph) and entangle (right graph) photon pair. H, V, D, D', R, L indicate horizontal, vertical, 2 diagonal, left circular and right circular polarizations. Right: Density matrices (real parts) of the these measurements and theoretical predictions. [Shields group, Nature 439, 179 (2006)]

Another interesting feature of quantum dots is their compatibility with current semiconductor technology. This allows their integration into electro-optical devices, such as light emitting diodes. In this way, electrically driven single-photon sources can be realized, an example of such a structure is shown in figure 164.

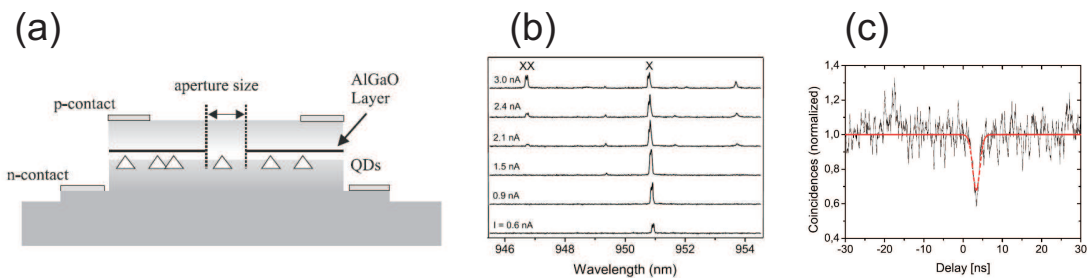


Figure 164: (a) Structure of a electrically pumped QD single-photon device. (b) Electroluminescence spectra at different current injection. (c) Autocorrelation measurement under continuous wave current injection (0.9 nA, 1.65 V) at 10 K. No spectral filtering was used to isolate a single transition in a single quantum dot. [HU+TU Berlin, Scholz et al., Opt. Express, 15, 9107 (2007)]

6.3.3 Colloidal Quantum Dots / Nanocrystals

Colloidal quantum dots also known as nanocrystals are (often spherical) core-shell heterostructures, that are chemically synthesized (see next chapter “Fabrication”) and that are available in colloidal solutions (figure 165). As a result of the synthesis, nanocrystals are usually additionally covered with a layer of organic ligands. Nanocrystals can be synthesized with a comparably high size uniformity and with a large size range which in turn allows access to broad wavelength range (see figure 165(c)). When spin-coating droplets of this colloid on a clean substrate one can prepare samples of low-density nanocrystals on a surface.

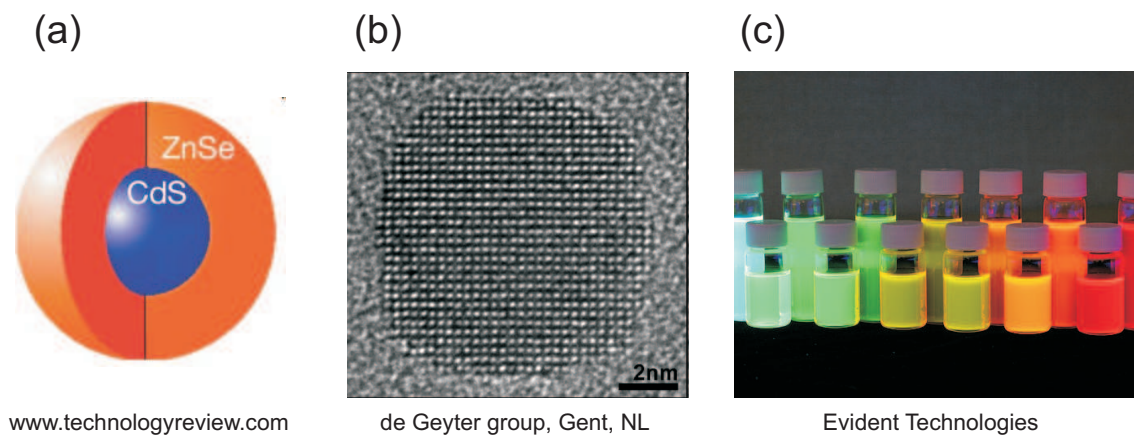


Figure 165: (a) Basic structure of a core-shell nanocrystal. (b) TEM image of a PbSe nanocrystal. (c) Colloidal solutions of CdSe/ZnSe nanocrystals with different sizes.

From their physical structure, nanocrystals are also semiconductor quantum dots, but are treated here separately as they possess different properties as compared to the epitaxial ones:

- Nanocrystals have a much higher quantum yield at room temperature (e.g. 97% reported in PRL 93, 107403 (2004)) due to the stronger confinement potential, with the absence of a wetting layer.
- Auger processes are much more efficient in nanometre-sized structures than in bulk materials. If the nanocrystal contains more than a single electron/hole pair non-radiative Auger recombination is often the preferential energy relaxation channel, thus suppressing radiative recombinations of higher excitations (see figure 166).

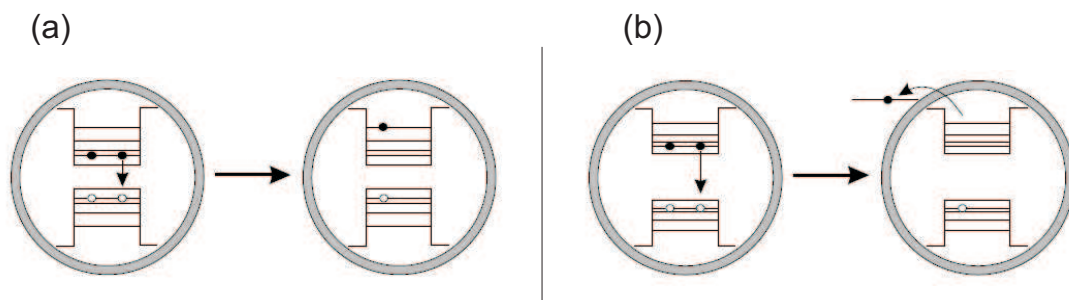


Figure 166: Principle of Auger recombination. The recombination energy is transferred to a remaining carrier. (a) Auger relaxation of a biexciton in a neutral nanocrystal. The remaining excited carrier is still confined in the nanocrystal. (b) Autoionization of a neutral nanocrystal. The remaining excited carrier is ejected from the QD. [Brokmann et al., *New. J. Phys.* 6, 99 (2004)].

- Due to the large surface–volume ratio, imperfect surfaces and the presence of organic ligands, surface traps for charge carriers can be populated, e.g., via Auger processes. The resulting charging can cause the nanocrystal to remain in a dark, non-radiative state over longer periods of time. The implication of this is a statistical *on–off* switching of the emission, which is called *blinking* (see figure 167) and which reduces their overall quantum efficiency.
- Nanocrystals are also subject to photo-bleaching.

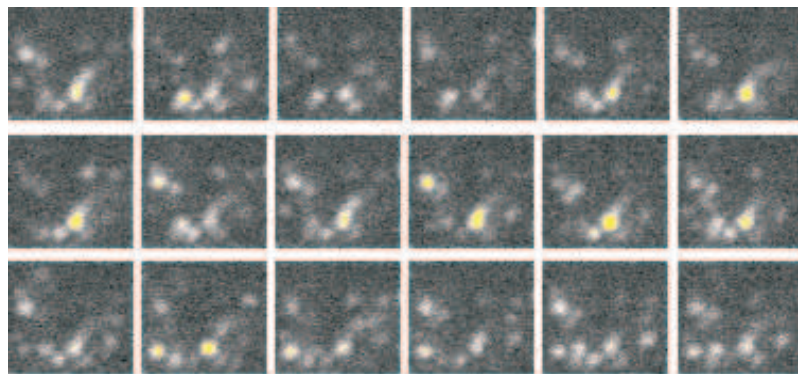
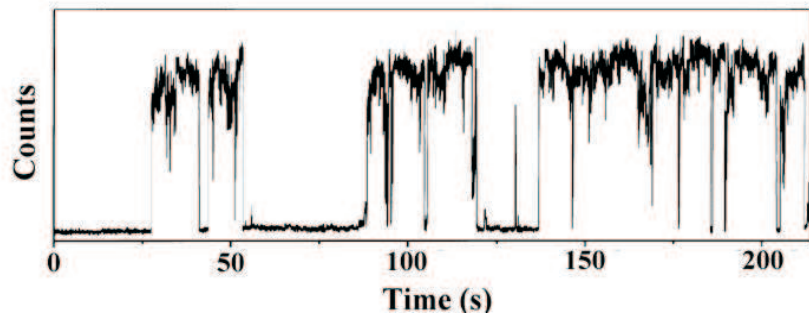


Figure 167: Blinking of nanocrystals. Top: time trace of the intensity of a single CdSe/ZnS nanocrystal [Bawendi group, MIT, Nirmal et al., Nature 383, 802 (1996)]. Bottom: Microscope image of several CdSe/ZnS nanocrystals. The subsequent images are taken in 100-ms steps from left to right and from top to bottom [HU Berlin + Univ. Hamburg].

6.3.4 Fluorescent Molecules

For an organic molecule, the lowest electronic transition appears between the *highest occupied molecular orbital* (HOMO) and the *lowest unoccupied molecular orbital* (LUMO). In addition, vibrational degrees of freedom have to be taken into account. For molecules, the electronic states have a manifold (harmonic oscillator-like) vibrational states superimposed. A typical energy level diagram of an organic molecule is depicted in figure 168.

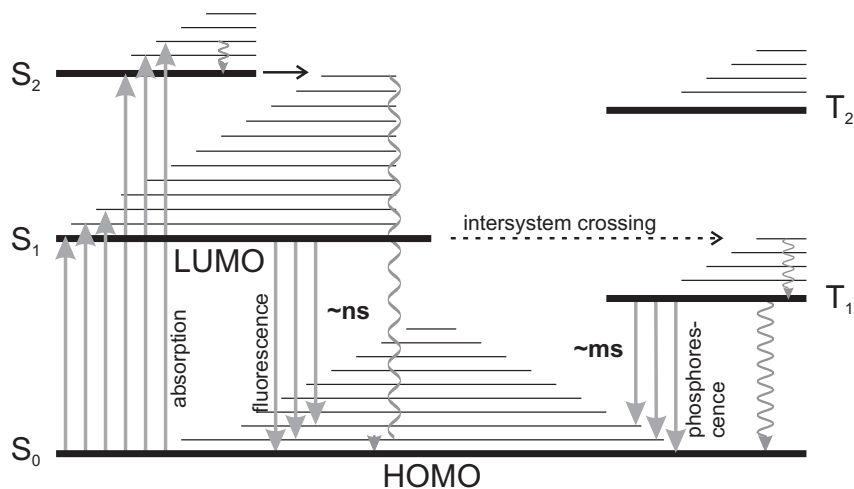


Figure 168: Energy level diagram of an organic molecule and different possible transitions. $S_{0,1,2,\dots}$: electronic singlet states, $T_{1,2,\dots}$: triplet states. Radiative transitions draw as solid lines, vibrational transitions as wavy lines. [Inspired from Novotny & Hecht, “Principles of Nano-Optics”]

The following transitions can occur:

- **Absorption:** Excitation of the molecule can be resonant into the vibrational ground state of the LUMO, non-resonant into higher vibrational modes of the LUMO or into higher excited electronic singlet states.
- **Vibrational relaxation:** This happens over fast decay cascades, which (for “good” chromophores) ends in the vibrational ground states. This happens on typical time scales of 1–1000 ps.
- **Fluorescence:** Radiative relaxation from the LUMO is called fluorescence. As the radiative lifetimes (0.1–1000 ns) for fluorescence are typically much larger than vibrational relaxation, these transitions usually only appear from the vibrational ground state of the LUMO (Kasha rule). However, the transitions

can also occur into higher vibrational states of the HOMO (which subsequently nonradiatively relax to the HOMO ground state). This leads to several spectral lines in the fluorescence spectrum.

- **Non-radiative decay from the LUMO to the HOMO.** This process competes with the radiative fluorescence. The ratio of the radiative decay rate γ_r an the total decay rate $\gamma_{tot} = \gamma_r + \gamma_{nr}$ is denoted as the quantum efficiency

$$\eta = \frac{\gamma_r}{\gamma_r + \gamma_{nr}}$$

where γ_{nr} is the non-radiative decay rate.

- **Phosphorescence:** Due to finite spin-orbit coupling in molecules there is a small but significant probability that the spin is reversed and the molecule transforms into a metastable triplet state. These states have comparably long lifetime (\approx ms). During this time the molecule is in a dark state. The on-off behaviour is called *blinking*. Radiative transitions from this state are called phosphorescence.

Typically a molecule eventually ceases to fluoresce completely, due to chemical reactions, such as oxidation. This process is called *photo-bleaching*.

As single molecules have discrete transitions, they can be employed as single-photon sources as well. In contrast to quantum dots, this can even occur at room temperature (see fig 169, but with the drawback of blinking/bleaching effects).

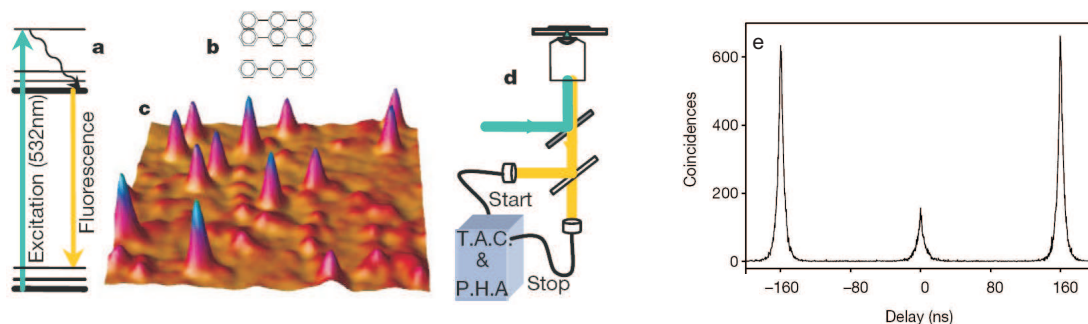


Figure 169: Single photon emission from a single molecule at room temperature. (a) Pumping scheme of the molecules to their fluorescent state. (b) Chemical structures of the emitter, terylene (upper structure), and its matrix, and p-terphenyl (lower structure). (c) Confocal fluorescence image ($10 \text{ mm} \times 10 \text{ mm}$) of single terylene molecules embedded in crystalline p-terphenyl with continuous-wave excitation at 532 nm. (d) Schematic representation of the scanning confocal microscope set-up used to characterize the single-molecule emission. (e) Second-order intensity correlation function of the emitted photons. [Lounis & Moerner, Nature 407, 491 (2000)]

6.3.5 Defects in Bulk or Nanocrystalline Diamonds

Diamond crystals can include a multitude of different defects, that either can exist naturally or can be introduced using ion implantation techniques.

The most prominent defect is the Nitrogen–Vacancy centre, in which two neighbouring carbon atoms are replaced by one nitrogen atom and a vacancy (figure 170(a)). Especially the charged NV^- -centre with an additional electron is of special interest in quantum information processing. This charged state is often referred to as the *NV centre* (NVC).

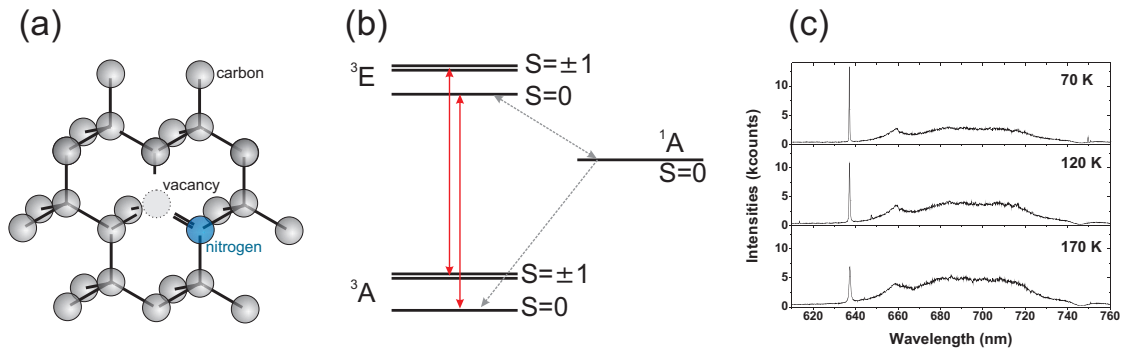


Figure 170: (a) Atomic structure of a NV defect in diamond. (b) Energy term scheme of a negatively charged NVC. (c) Fluorescence images of a single bulk NVC taken at different temperatures [HU Berlin].

The energy level structure of an NVC is shown in figure 170(b). With an even number of electrons the NVC has an integer spin. It was found that the ground state is formed by a triplet state 3A . There are two excited states, a bright triplet state 3E and a metastable singlet state 1A with lower energy (the number indicates the number of spin states $M = 2S + 1$). The $S_z = 0$ and $S_z = \pm 1$ sublevels of the triplet states are split in the GHz regime due to spin–orbit and spin–spin coupling. The singlet state can be populated by spin-flip processes.

The transition from the ground-state to the excited state has a zero-phonon excitation line of 637 nm, so that the NVC can be pumped optically. Because of large coupling to phonon sidebands, the transition can be pumped via green light (e.g. 532 nm), and when the system relaxes back to its ground-state the NVC emits broadband red light. The lifetime of the excited state in bulk diamond is 12.9 ns. Spectra taken at different temperatures on a single bulk NVC are shown in figure 170(c).

NVCs are well suited for single-photon sources, as long as short wavepackets and narrow, Fourier limited spectra are not required. NVCs allow efficient and stable (no blinking/bleaching) single-photon emission already at room temperature as shown in figure 171. As NVCs are also found in diamond nanocrystals, that can be freely positioned using nanomanipulation techniques, or prepared as low-density samples. NVCs are also interesting candidates for qubits in quantum information processing, as the magnetic sublevels can be coherently controlled using optical and microwave transitions.

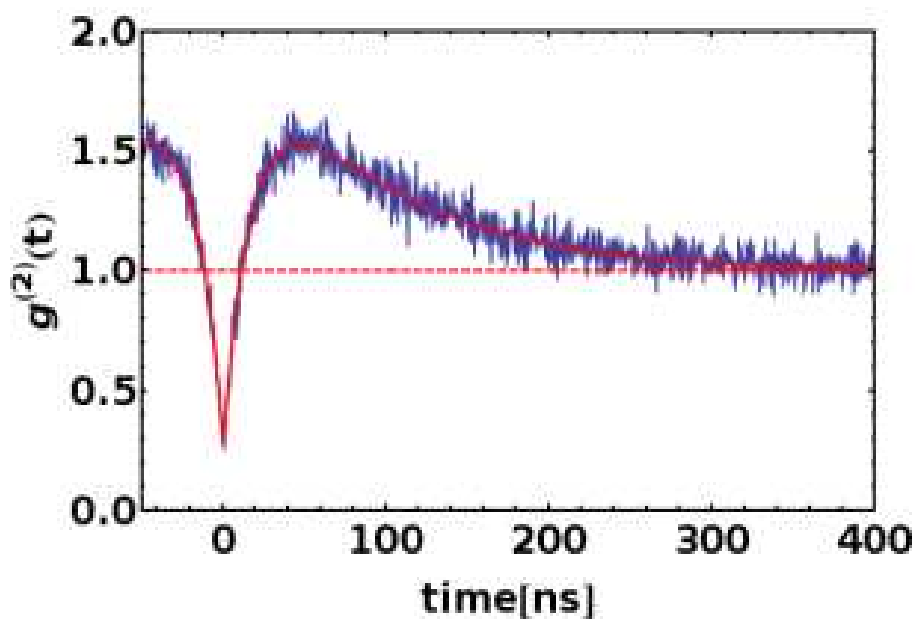


Figure 171: Anti-bunching observed in the photon correlation of fluorescence light from a single NV center at room temperature.